Progress In Electromagnetics Research, PIER 27, 61–89, 2000

NEAR ELECTROMAGNETIC FIELDS IN OPEN CHIROSTRIP STRUCTURES EXCITED BY PRINTED DIPOLES

F. Lumini

EMBRAER S. A.
Division of Systems Engineering
Av. Brig. Faria Lima, 2170
12227-901 São José dos Campos, SP - Brazil

J. C. da S. Lacava

Instituto Tecnológico de Aeronáutica
Department of Electronic Engineering
Praça Mal. Eduardo Gomes, 50
12228-900 São José dos Campos, SP - Brazil

1. INTRODUCTION

During the last ten years, special attention has been focused on electromagnetic chirality and its potential application in the design of new devices and components. The reflection and transmission processes for semi-infinite chiral media and for infinite chiral slabs have been analyzed by Bassari, Papas, and Engheta [1]. The theory of electromagnetic wave propagation in cylindrical waveguides containing chiral materials, termed chirowaveguides, has been presented and discussed by Pelet and Engheta [2, 3]. Open chirowaveguides, another class of waveguiding structures with chiral material, have been the subject of studies of several researchers [4–6]. Mariotte, Pelet and Engheta presented an excellent review of guided waves [7], and some canonical problems whose solution may eventually result in useful chiral devices were reviewed by Cory [8]. In 1997, Lacava and Lumini proposed an alternative formulation for guided electromagnetic fields in grounded chiral slabs [9]. More recently, the dispersion characteristics of fundamental modes of planar chiral lines have been studied by Plaza, Mesa and Horno [10].

The use of chiral media in microstrip antennas has also been discussed. Effects of chiral admittance in the radiation pattern and in the surface-wave power excited by chirostrip line antennas were studied and reported in [11]. The electromagnetic fields radiated by chirostrip printed dipoles were also analyzed by many authors (e.g., [12–16], just to mention a few). Specifically, the possibility of rotating the radiation patterns was presented by Pelet and Engheta [17]. The current distribution, input impedance, mutual coupling, bandwidth, and efficiency of cylindrical chirostrip antennas were investigated in [15, 18]. On the other hand, works on the analysis of microstrip patch antennas and infinite arrays on chiral substrate have been carried out by Pozar [19] and by Toscano and Legni [20]. In spite of numerous works published on chirostrip structure [21–23], there is not enough information about the numerical calculation of near electromagnetic field distribution in chirostrip antennas.

Using a full-wave spectral-domain analysis method, this paper presents a dynamic model to calculate the near electromagnetic fields excited by a short dipole printed on a grounded chiral slab. This means that the fields in the space domain are obtained through double integrals in the Fourier domain. As the antenna is printed on the planar interface that separates the chiral substrate from the free space region,

the calculations of the electromagnetic fields involve Sommerfeld type integrals. If the observation point is far from the interface, these integrals include exponentially decaying terms in the integrand which facilitate convergence. On the other hand, if the observation point is on the interface, these integrals converge very slowly. Consequently, special considerations are required in this case. First of all, we carry out a transformation from rectangular into polar coordinates in the $k_x - k_y$ spectral plane using the following formulas: $k_x = \beta\cos(\alpha)$ and $k_y = \beta\sin(\alpha)$. Then, we do another rectangular to polar transformation, this time in the x-y space domain: $x = \rho\cos(\phi)$ and $y = \rho\sin(\phi)$. This procedure allows, in general, to solve analytically the integrals in α. The integrals in β, however, must be evaluated numerically. To exemplify the procedure, the calculation of the x-component of the electric field in the chiral substrate and in the free space region is discussed in detail.

Using this approach, the effects of chirality on near electromagnetic field distributions are analyzed. It has been observed that the chirality causes a rotation in the near-field patterns. This phenomenon has been reported only for the far field region [17]. As expected, our calculation confirms that the behavior of the magnetic field at the chirostrip antenna interfaces is different from that usually observed in microstrip antennas.

2. THEORY

Fig. 1 shows the geometry of the problem. A homogeneous isotropic linear chiral medium, having thickness d, permittivity ε_c, permeability μ_0 (non-magnetic substrate), and chiral admittance ξ_c, lies on an infinite perfectly conducting plate located on the x-y plane of a rectangular coordinate system. The planar interface $z = d$ separates the chiral substrate $(0 < z < d)$ from the free space region $(z > d$, permittivity ε_0 and permeability $\mu_0)$. For a lossless chiral substrate, the parameters ε_c and ξ_c are real quantities. The x-directed short dipole is printed on the planar interface at the position $x = 0$, $y = 0$, and $z = d$. As the chiral medium is isotropic, the choice of the dipole direction does not pose any restriction on the present discussion.

The theory used in this work treats the structure as a boundary value problem where the short dipole current is the virtual source of the electromagnetic fields. In our approach, the wave equations in the chiral layer and in the free-space region are solved in the Fourier do-

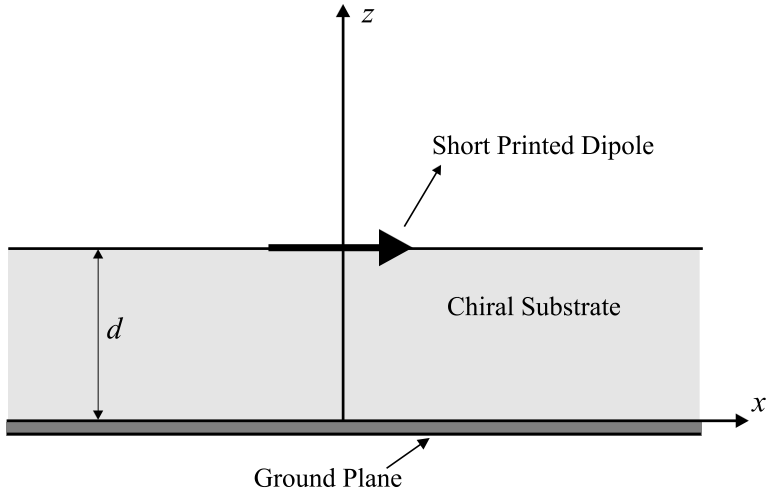

Figure 1. X-directed short dipole printed on a grounded chiral slab.

main. This technique effectively removes the singularity of the spatial Green functions and allows considerable simplification in the method of moment calculations [24]. After that, the boundary conditions for the electromagnetic fields are applied on the interfaces $z = 0$ and $z = d$, resulting in a set of six equations with six unknowns. The spectral fields at any point of region $z \geq 0$ are determined by solving this set of equations. Finally, the electromagnetic fields in the space domain are obtained through the application of the inverse Fourier transform.

3. ELECTROMAGNETIC FIELDS IN THE CHIRAL SUBSTRATE

In this section, expressions for electromagnetic fields inside the chiral substrate are derived. For time-harmonic variations, assuming time dependence of the form $e^{i\omega t}$, Maxwell's equations for source-free media are given by

$$\nabla \times \vec{\mathbf{E}}(x, y, z) = -i\omega\vec{\mathbf{B}}(x, y, z) \tag{1}$$

$$\nabla \times \vec{\mathbf{H}}(x, y, z) = i\omega\vec{\mathbf{D}}(x, y, z) \tag{2}$$

$$\nabla \cdot \vec{\mathbf{D}}(x, y, z) = 0 \tag{3}$$

$$\nabla \cdot \vec{\mathbf{B}}(x, y, z) = 0. \tag{4}$$

Using the Post-Jaggard time-harmonic constitutive relations [25],

$$\vec{\mathbf{D}}(x,y,z) = \varepsilon_c \vec{\mathbf{E}}(x,y,z) - i\xi_c \vec{\mathbf{B}}(x,y,z) \tag{5}$$

$$\vec{\mathbf{B}}(x,y,z) = \mu_0 \vec{\mathbf{H}}(x,y,z) + i\mu_0 \xi_c \vec{\mathbf{E}}(x,y,z) \tag{6}$$

the wave equation for the electric field inside the chiral substrate can be written as

$$\nabla^2 \vec{\mathbf{E}}(x,y,z) + 2p\nabla \times \vec{\mathbf{E}}(x,y,z) + k_c^2 \vec{\mathbf{E}}(x,y,z) = 0 \tag{7}$$

where $k_c^2 = \omega^2 \mu_0 \varepsilon_c$ and $p = \omega \mu_0 \xi_c$.

As the geometry shown in Fig. 1 is unbounded in the x and y directions, we use in our calculations the expression

$$\vec{\boldsymbol{\mathcal{E}}}(k_x, k_y, z) = \iint_{-\infty}^{+\infty} \vec{\mathbf{E}}(x,y,z) e^{i(k_x x + k_y y)} dx dy \tag{8}$$

for the double Fourier transform of the electric field $\vec{\mathbf{E}}(x,y,z)$.

If we Fourier transform the wave equation (7) and the solutions for the transformed electric field components are expressed in the form

$$\boldsymbol{\mathcal{E}}_\eta(k_x, k_y, z) = \mathbf{e}_\eta(k_x, k_y) e^{i\gamma z} \tag{9}$$

where $\mathbf{e}_\eta(k_x, k_y)$ are functions to be determined $(\eta = x, y \text{ or } z)$, the following biquadratic equation can be obtained

$$\gamma^4 - 2\gamma^2(k_c^2 + 2p^2 - u^2) + k_c^4 + u^4 - 2k_c^2 u^2 - 4p^2 u^2 = 0 \tag{10}$$

where $u^2 = k_x^2 + k_y^2$.

Solving this equation, four different propagation constants are determined:

$$\gamma_1 = \sqrt{k_+^2 - u^2} \tag{11}$$

$$\gamma_2 = \sqrt{k_-^2 - u^2} \tag{12}$$

$$\gamma_3 = -\gamma_1 \tag{13}$$

$$\gamma_4 = -\gamma_2 \tag{14}$$

where $k_+ = q + p$, $k_- = q - p$ and $q = (k_c^2 + p^2)^{1/2}$. According to [17], k_+ and k_- are the wavenumbers of the right- and left-circulary polarized waves propagating in an unbounded chiral medium.

Considering the solutions (11)–(14), we can write the expressions for the transformed electric field components inside the chiral substrate in the following way

$$\boldsymbol{\mathcal{E}}_\eta(k_x, k_y, z) = \sum_{\tau=1}^{4} \mathbf{e}_{\eta_\tau}(k_x, k_y) e^{i\gamma_\tau z}. \tag{15}$$

Using a similar procedure, the components of magnetic field are given by

$$\boldsymbol{\mathcal{H}}_\eta(k_x, k_y, z) = \sum_{\tau=1}^{4} \mathbf{h}_{\eta_\tau}(k_x, k_y) e^{i\gamma_\tau z}. \tag{16}$$

At this point, we have twenty four unknowns: the functions $\mathbf{e}_{\eta_\tau}(k_x, k_y)$ and $\mathbf{h}_{\eta_\tau}(k_x, k_y)$ with $\tau = 1, 2, 3$ or 4 and $\eta = x, y$ or z.

The expressions for the electromagnetic fields in the space domain are obtained through the inverse Fourier transform of $\vec{\boldsymbol{\mathcal{E}}}(k_x, k_y, z)$ and $\vec{\boldsymbol{\mathcal{H}}}(k_x, k_y, z)$. For the τ-th solution of γ and the η-th component of the electric field, we have

$$\mathbf{E}_{\eta_\tau}(x, y, z) = \frac{1}{4\pi^2} \iint_{-\infty}^{+\infty} \mathbf{e}_{\eta_\tau}(k_x, k_y) e^{-i(k_x x + k_y y - \gamma_\tau z)} dk_x dk_y. \tag{17}$$

Introducing the expressions for the inverse Fourier transform of $\vec{\boldsymbol{\mathcal{E}}}(k_x, k_y, z)$ and $\vec{\boldsymbol{\mathcal{H}}}(k_x, k_y, z)$ in the Maxwell's equations (1) and (2), we can write $\mathbf{e}_{x_\tau}(k_x, k_y)$, $\mathbf{e}_{y_\tau}(k_x, k_y)$, $\mathbf{h}_{x_\tau}(k_x, k_y)$, $\mathbf{h}_{y_\tau}(k_x, k_y)$, and $\mathbf{h}_{z_\tau}(k_x, k_y)$ as functions of $\mathbf{e}_{z_\tau}(k_x, k_y)$:

$$\mathbf{e}_{x_\tau}(k_x, k_y) = \frac{1}{u^2} \left[\gamma_\tau k_x + i(-1)^\tau k_\tau k_y\right] \mathbf{e}_{z_\tau}(k_x, k_y) \tag{18}$$

$$\mathbf{e}_{y_\tau}(k_x, k_y) = \frac{1}{u^2} \left[i(-1)^{\tau+1} k_\tau k_x + \gamma_\tau k_y\right] \mathbf{e}_{z_\tau}(k_x, k_y) \tag{19}$$

$$\mathbf{h}_{x_\tau}(k_x, k_y) = \frac{q}{\omega\mu_0 u^2} \left[i(-1)^{\tau+1} \gamma_\tau k_x + k_\tau k_y\right] \mathbf{e}_{z_\tau}(k_x, k_y) \tag{20}$$

$$\mathbf{h}_{y_\tau}(k_x, k_y) = \frac{q}{\omega\mu_0 u^2} \left[-k_\tau k_x + i(-1)^{\tau+1} \gamma_\tau k_y\right] \mathbf{e}_{z_\tau}(k_x, k_y) \tag{21}$$

$$\mathbf{h}_{z_\tau}(k_x, k_y) = (-1)^{\tau+1} \frac{iq}{\omega\mu_0} \mathbf{e}_{z_\tau}(k_x, k_y) \tag{22}$$

where $k_1 = k_3 = k_+$ and $k_2 = k_4 = k_-$. With the procedure just described, we have drastically reduced the number of unknowns in the chiral substrate. There are now only four unknowns: the functions $\mathbf{e}_{z_1}(k_x, k_y)$, $\mathbf{e}_{z_2}(k_x, k_y)$, $\mathbf{e}_{z_3}(k_x, k_y)$ and $\mathbf{e}_{z_4}(k_x, k_y)$.

4. ELECTROMAGNETIC FIELDS IN THE FREE SPACE

The wave equation for the electric field in the free space $(z > d)$ can be obtained from equation (7) if the particular conditions $\xi_c = 0$ and $\varepsilon_c = \varepsilon_0$ are observed. After the substitution of these values, we have

$$\nabla^2 \vec{\mathbf{E}}_0(x, y, z) + k_0^2 \vec{\mathbf{E}}_0(x, y, z) = 0 \tag{23}$$

where $k_0^2 = \omega^2 \mu_0 \varepsilon_0$.

Using a procedure similar to that presented in the previous section, the expressions for the transformed electromagnetic field components in the free space are given by

$$\boldsymbol{\mathcal{E}}_{\eta_0}(k_x, k_y, z) = \mathbf{e}_{\eta_0}(k_x, k_y) e^{-ik_{z0}z} \tag{24}$$

$$\boldsymbol{\mathcal{H}}_{\eta_0}(k_x, k_y, z) = \mathbf{h}_{\eta_0}(k_x, k_y) e^{-ik_{z0}z} \tag{25}$$

where $k_{z0} = (k_0^2 - u^2)^{1/2}$. We have eliminated the wave propagating toward negative z because this region is unbounded for $z > d$.

Consequently, the functions $\mathbf{e}_{x_0}(k_x, k_y)$, $\mathbf{e}_{y_0}(k_x, k_y)$, $\mathbf{h}_{x_0}(k_x, k_y)$, and $\mathbf{h}_{y_0}(k_x, k_y)$ can be written as functions of $\mathbf{e}_{z_0}(k_x, k_y)$, as follows

$$\mathbf{e}_{x_0}(k_x, k_y) = -u^{-2} \left[k_x k_{z0} \mathbf{e}_{z_0}(k_x, k_y) + \omega \mu_0 k_y \mathbf{h}_{z_0}(k_x, k_y) \right] \tag{26}$$

$$\mathbf{e}_{y_0}(k_x, k_y) = -u^{-2} \left[k_y k_{z0} \mathbf{e}_{z_0}(k_x, k_y) - \omega \mu_0 k_x \mathbf{h}_{z_0}(k_x, k_y) \right] \tag{27}$$

$$\mathbf{h}_{x_0}(k_x, k_y) = -u^{-2} \left[-\omega \varepsilon_0 k_y \mathbf{e}_{z_0}(k_x, k_y) + k_x k_{z0} \mathbf{h}_{z_0}(k_x, k_y) \right] \tag{28}$$

$$\mathbf{h}_{y_0}(k_x, k_y) = -u^{-2} \left[\omega \varepsilon_0 k_x \mathbf{e}_{z_0}(k_x, k_y) + k_y k_{z0} \mathbf{h}_{z_0}(k_x, k_y) \right]. \tag{29}$$

So, in the free space we have only two unknowns $\mathbf{e}_{z_0}(k_x, k_y)$ and $\mathbf{h}_{z_0}(k_x, k_y)$.

In summary, the total number of unknowns in this formulation is six. These unknowns will be found by applying the boundary conditions for the electromagnetic fields on the interfaces of the chirostrip structure.

5. BOUNDARY CONDITIONS

For the geometry presented in Fig. 1, the necessary and sufficient boundary conditions are those that require the tangential components of the electric field to vanish on the ground plane $(z = 0)$, the continuity of the tangential components of the electric field on the chiral-free space interface $z = d$, and the discontinuity of the tangential components of the magnetic field on the same interface due to the printed dipole. After the application of these conditions, we can write the following system of equation involving $\mathbf{e}_{z_\tau}(k_x, k_y)$, $\mathbf{e}_{z_0}(k_x, k_y)$, and $\mathbf{h}_{z_0}(k_x, k_y)$:

$$\sum_{\tau=1}^{4} [\gamma_\tau \mathbf{e}_{z_\tau}(k_x, k_y)] = 0 \tag{30}$$

$$\sum_{\tau=1}^{4} [(-1)^\tau k_\tau \mathbf{e}_{z_\tau}(k_x, k_y)] = 0 \tag{31}$$

$$\sum_{\tau=1}^{4} \left[\gamma_\tau e^{i\gamma_\tau d} \mathbf{e}_{z_\tau}(k_x, k_y)\right] + k_{z0} e^{-ik_{z0}d} \mathbf{e}_{z_0}(k_x, k_y) = 0 \tag{32}$$

$$\sum_{\tau=1}^{4} \left[(-1)^\tau k_\tau e^{i\gamma_\tau d} \mathbf{e}_{z_\tau}(k_x, k_y)\right] - i\omega\mu_0 e^{-ik_{z0}d} \mathbf{h}_{z_0}(k_x, k_y) = 0 \tag{33}$$

$$\sum_{\tau=1}^{4} \left[(-1)^{\tau+1} q\gamma_\tau e^{i\gamma_\tau d} \mathbf{e}_{z_\tau}(k_x, k_y)\right] - ik_{z0}\omega\mu_0 e^{-ik_{z0}d} \mathbf{h}_{z_0}(k_x, k_y) = -i\boldsymbol{I}\omega\mu_0 k_y \tag{34}$$

$$\sum_{\tau=1}^{4} \left[qk_\tau e^{i\gamma_\tau d} \mathbf{e}_{z_\tau}(k_x, k_y)\right] - k_0^2 e^{-ik_{z0}d} \mathbf{e}_{z_0}(k_x, k_y) = -\boldsymbol{I}\omega\mu_0 k_x \tag{35}$$

where $\boldsymbol{I}$, a constant expressed in ampere $\cdot$ meters, is the Fourier transform of the current on the short dipole.

Solving the system (30)–(35), the functions $\mathbf{e}_{z_\tau}(k_x, k_y)$, $\mathbf{e}_{z_0}(k_x, k_y)$, and $\mathbf{h}_{z_0}(k_x, k_y)$ are finally determined. Inserting these functions into equations (18)–(22) and (26)–(29), and then into equations (15), (16), (24), and (25), we obtain the expressions for the components of the transformed electromagnetic fields inside and outside the chiral substrate. The expressions for the x-component of the transformed electric field are presented below and those for the other components are listed in the Appendix.

Inside the chiral substrate $(0 < z < d)$, we have:

$$\boldsymbol{\mathcal{E}}_x(k_x, k_y, z) = \frac{\omega \boldsymbol{I} \mu_0}{2u^2 \Delta(u^2)} \Big[M_{xx}^{(c)}(z, u^2) k_x^2 + M_{xy}^{(c)}(z, u^2) k_x k_y + M_{yy}^{(c)}(z, u^2) k_y^2 \Big] \tag{36}$$

where

$$\begin{aligned}
M_{xx}^{(c)}(z, u^2) &= [\cos(\gamma_1 z) - \cos(\gamma_2 z)]\, A_x \\
&\quad - iz \left[k_- \gamma_1^2 \operatorname{sinc}(\gamma_1 z) + k_+ \gamma_2^2 \operatorname{sinc}(\gamma_2 z) \right] B_x && (37) \\
M_{xy}^{(c)}(z, u^2) &= (A_y + i k_c^2 B_x) \left[\cos(\gamma_1 z) - \cos(\gamma_2 z) \right] \\
&\quad + z \left[k_+ A_x - i k_- \gamma_1^2 B_y \right] \operatorname{sinc}(\gamma_1 z) \\
&\quad + z \left[k_- A_x - i k_+ \gamma_2^2 B_y \right] \operatorname{sinc}(\gamma_2 z) && (38) \\
M_{yy}^{(c)}(z, u^2) &= i k_c^2 \left[\cos(\gamma_1 z) - \cos(\gamma_2 z) \right] B_y \\
&\quad + z \left[k_+ \operatorname{sinc}(\gamma_1 z) + k_- \operatorname{sinc}(\gamma_2 z) \right] A_y && (39) \\
A_x &= k_{z0}^2 k_c^2 \left[\cos(\gamma_1 d) - \cos(\gamma_2 d) \right] \\
&\quad + i q k_{z0} d \left[k_- \gamma_1^2 \operatorname{sinc}(\gamma_1 d) - k_+ \gamma_2^2 \operatorname{sinc}(\gamma_2 d) \right] && (40) \\
A_y &= - i q k_{z0} k_c^2 \Big[\cos(\gamma_1 d) + \cos(\gamma_2 d) \Big] \\
&\quad + k_0^2 d \left[k_- \gamma_1^2 \operatorname{sinc}(\gamma_1 d) + k_+ \gamma_2^2 \operatorname{sinc}(\gamma_2 d) \right] && (41) \\
B_x &= q k_{z0} \left[\cos(\gamma_1 d) + \cos(\gamma_2 d) \right] \\
&\quad + i k_{z0}^2 d \left[k_+ \operatorname{sinc}(\gamma_1 d) + k_- \operatorname{sinc}(\gamma_2 d) \right] && (42) \\
B_y &= i k_0^2 \left[- \cos(\gamma_1 d) + \cos(\gamma_2 d) \right] \\
&\quad + q k_{z0} d \left[k_+ \operatorname{sinc}(\gamma_1 d) - k_- \operatorname{sinc}(\gamma_2 d) \right] && (43) \\
\Delta(u^2) &= k_c^2 k_{z0} (q^2 + k_0^2) \cos(\gamma_1 d) \cos(\gamma_2 d) \\
&\quad + i q d (k_0^2 \gamma_2^2 k_+ + k_{z0}^2 k_c^2 k_-) \cos(\gamma_1 d) \operatorname{sinc}(\gamma_2 d) \\
&\quad + i q d (k_{z0}^2 k_c^2 k_+ + k_0^2 \gamma_1^2 k_-) \operatorname{sinc}(\gamma_1 d) \cos(\gamma_2 d) \\
&\quad - 0.5 d^2 k_{z0} (k_+^2 \gamma_2^2 + k_-^2 \gamma_1^2)(q^2 + k_0^2) \operatorname{sinc}(\gamma_1 d) \operatorname{sinc}(\gamma_2 d) \\
&\quad + k_c^2 k_{z0} (q^2 - k_0^2) && (44) \\
\operatorname{sinc}(x) &= \sin(x)/x && (45)
\end{aligned}$$

In the free space $(z > d)$, we have:

$$\boldsymbol{\mathcal{E}}_{x_0}(k_x, k_y, z) = \frac{\omega \boldsymbol{I} \mu_0 e^{i k_{z0}(d-z)}}{u^2 \Delta(u^2)} \Big[M_{xx}^{(0)}(u^2) k_x^2 + M_{xy}^{(0)}(u^2) k_x k_y + M_{yy}^{(0)}(u^2) k_y^2 \Big] \tag{46}$$

where

$$\begin{aligned} M_{xx}^{(0)}(u^2) = {} & k_c^2 k_{z0}^2 \left[1 - \cos(\gamma_1 d)\cos(\gamma_2 d)\right] \\ & - iqdk_{z0}\left[k_+\gamma_2^2 \cos(\gamma_1 d)\,\mathrm{sinc}(\gamma_2 d)\right. \\ & \left. + \; k_-\gamma_1^2 \cos(\gamma_2 d)\,\mathrm{sinc}(\gamma_1 d)\right] \\ & + 0.5d^2 k_{z0}^2 (k_+^2\gamma_2^2 + k_-^2\gamma_1^2)\,\mathrm{sinc}(\gamma_1 d)\,\mathrm{sinc}(\gamma_2 d) \end{aligned} \tag{47}$$

$$M_{xy}^{(0)}(u^2) = 4ipd^2q^2u^2k_{z0}\,\mathrm{sinc}(\gamma_1 d)\,\mathrm{sinc}(\gamma_2 d) \tag{48}$$

$$\begin{aligned} M_{yy}^{(0)}(u^2) = {} & k_c^2 k_0^2 \left[1 - \cos(\gamma_1 d)\cos(\gamma_2 d)\right] \\ & - iqdk_{z0}k_c^2\left[k_- \cos(\gamma_1 d)\,\mathrm{sinc}(\gamma_2 d)\right. \\ & \left. + \; k_+ \cos(\gamma_2 d)\,\mathrm{sinc}(\gamma_1 d)\right] \\ & + 0.5d^2 k_0^2 (k_+^2\gamma_2^2 + k_-^2\gamma_1^2)\,\mathrm{sinc}(\gamma_1 d)\,\mathrm{sinc}(\gamma_2 d) \end{aligned} \tag{49}$$

6. COMPUTATION OF NEAR ELECTROMAGNETIC FIELDS

Since the electromagnetic fields in the space domain are obtained applying the inverse Fourier transform to the expressions of the transformed fields, double integrals in the spectral variables k_x and k_y must be calculated. To exemplify this procedure, we will discuss here in detail only the calculation of the electric field component $\mathbf{E}_x(x, y, z)$ in the chiral substrate. This component is given by:

$$\begin{aligned} \mathbf{E}_x(x,y,z) = \frac{\omega \boldsymbol{I}\mu_0}{8\pi^2} \int_{-\infty}^{+\infty} \int \frac{1}{u^2\Delta(u^2)} \Big[& M_{xx}^{(c)}(z,u^2)k_x^2 + M_{xy}^{(c)}(z,u^2)k_xk_y \\ & + \; M_{yy}^{(c)}(z,u^2)k_y^2\Big] e^{-i(k_x x + k_y y)} dk_x dk_y \end{aligned} \tag{50}$$

In order to evaluate the double integral in (50), first of all we carry out a transformation from rectangular into polar coordinates in the spectral domain using the following formulas: $k_x = \beta\cos(\alpha)$ and $k_y = \beta\sin(\alpha)$. Then, we do another rectangular-to-polar transformation, this time in the x-y plane: $x = \rho\cos(\phi)$ and $y = \rho\sin(\phi)$. This means that we move from rectangular to cylindrical coordinates in the space domain. Equation (50) can be now rewritten as

$$
\begin{aligned}
&\mathbf{E}_x(\rho,\phi,z)\\
&= \frac{\omega \boldsymbol{I}\mu_0}{8\pi^2}\int_0^{+\infty}\frac{\beta}{\Delta(\beta^2)}\Big\{\Big[M_{xx}^{(c)}(z,\beta^2)\cos^2(\phi)+M_{yy}^{(c)}(z,\beta^2)\sin^2(\phi)\\
&\quad + M_{xy}^{(c)}(z,\beta^2)\cos(\phi)\sin(\phi)\Big]\int_0^{2\pi}e^{-i\beta\rho\cos(\alpha)}d\alpha+\Big[M_{yy}^{(c)}(z,\beta^2)\cos(2\phi)\\
&\quad - M_{xx}^{(c)}(z,\beta^2)\cos(2\phi)-M_{xy}^{(c)}(z,\beta^2)\sin(2\phi)\Big]\int_0^{2\pi}\sin^2(\alpha)e^{-i\beta\rho\cos(\alpha)}d\alpha\\
&\quad +\Big[M_{yy}^{(c)}(z,\beta^2)\sin(2\phi)-M_{xx}^{(c)}(z,\beta^2)\sin(2\phi)\\
&\quad + M_{xy}^{(c)}(z,\beta^2)\cos(2\phi)\Big]\int_0^{2\pi}\cos(\alpha)\sin(\alpha)e^{-i\beta\rho\cos(\alpha)}d\alpha\Big\}d\beta
\end{aligned}
\tag{51}
$$

Considering the following identities [26]:

$$
\int_0^{2\pi}e^{-i\beta\rho\cos(\xi)}d\xi = 2\pi J_0(\beta\rho) \tag{52}
$$

$$
\int_0^{2\pi}\sin^2(\xi)e^{-i\beta\rho\cos(\xi)}d\xi = \frac{2\pi}{\beta\rho}J_1(\beta\rho) \tag{53}
$$

$$
\int_0^{2\pi}\cos(\xi)\sin(\xi)e^{-i\beta\rho\cos(\xi)}d\xi = 0 \tag{54}
$$

where $J_0(z)$ and $J_1(z)$ are Bessel functions of the first kind, the expression for the $\mathbf{E}_x(\rho,\phi,z)$ component is given by

$$
\mathbf{E}_x(\rho,\phi,z) = \int_0^{+\infty}F(\beta)d\beta \tag{55}
$$

where

$$F(\beta) = \frac{\omega \boldsymbol{I} \mu_0}{4\pi} \frac{\beta}{\Delta(\beta^2)} \left\{ \left[M_{xx}^{(c)}(z,\beta^2)\cos^2(\phi) + M_{yy}^{(c)}(z,\beta^2)\sin^2(\phi) + M_{xy}^{(c)}(z,\beta^2)\cos(\phi)\sin(\phi) \right] J_0(\beta\rho) + \left[M_{yy}^{(c)}(z,\beta^2)\cos(2\phi) - M_{xx}^{(c)}(z,\beta^2)\cos(2\phi) - M_{xy}^{(c)}(z,\beta^2)\sin(2\phi) \right] \frac{J_1(\beta\rho)}{\beta\rho} \right\} \quad (56)$$

is a complex function to be integrated. Note that we were able to solve analytically only the integral in α. The integral in β will be evaluated numerically.

To better understand the behavior of the complex function $F(\beta)$, we have drawn in Fig. 2 this function versus β for $f = 2.0\,\mathrm{GHz}$, $\boldsymbol{I} = 1.0\,\mathrm{milliampere.meter}$, $\varepsilon_c = 2.0\varepsilon_0$, $d = 32.0\,\mathrm{mm}$, $\xi_c = 1.0\,\mathrm{mS}$, $\rho = 3.0d$, $\phi = 90^\circ$, and $z = 0.8d$. An analysis of the complex function $F(\beta)$ shows that its real part (continuous line in Fig. 2) is different from zero only between 0 and k_0 ($k_0 = 41.917\,\mathrm{rad/m}$) and has a delta Dirac behavior at the pole position ($\beta_p = 54.263\,\mathrm{rad/m}$). The imaginary part of this function (dashed line in Fig. 2) is discontinuous at the pole position, has its first derivative also discontinuous at k_0, and shows an oscillatory behavior when $\beta \to +\infty$. We note that, as shown in [9], the pole is located between k_0 and k_+.

The computation of the integral of the complex function $F(\beta)$ is divided into 5 parts:

$$\int_0^{+\infty} F(\beta)d\beta = \int_0^{k_0} F(\beta)d\beta + \int_{k_0}^{\beta_p-\delta} F(\beta)d\beta + \int_{\beta_p-\delta}^{\beta_p+\delta} F(\beta)d\beta + \int_{\beta_p+\delta}^{b} F(\beta)d\beta + \int_{b}^{+\infty} F(\beta)d\beta \quad (57)$$

where β_p is the pole position and b is the first zero greater than k_+ of the imaginary part. We have only considered the condition of one pole. Increasing the chiral substrate thickness and/or the operation frequency, the complex function $F(\beta)$ can exhibit more than one pole.

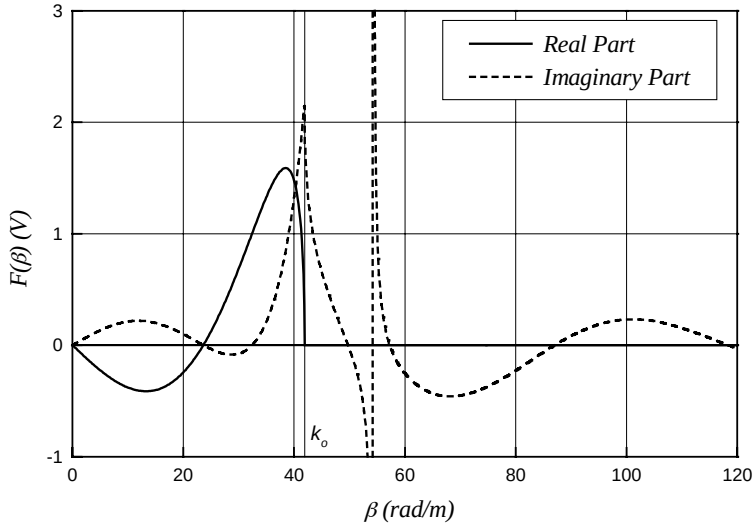

Figure 2. Complex function $F(\beta)$ that must be integrated to obtain the electric field component $\mathbf{E}_x(\rho, \phi, z)$ in the chiral substrate, computed for $f = 2.0\,\text{GHz}$, $\boldsymbol{I} = 1.0\,\text{milliampere.meter}$, $\varepsilon_c = 2.0\varepsilon_0$, $d = 32.0\,\text{mm}$, $\xi_c = 1.0\,\text{mS}$, $\rho = 3.0d$, $\phi = 90°$, and $z = 0.8d$.

In this case, additional terms must be added to the expression (57).

- Calculation of $\int_0^{k_0} F(\beta)d\beta$

In this interval, the function to be integrated has both the real and the imaginary parts. The integrals are calculated numerically using the DQDAGS subroutine available in the IMLS mathematical package version 10. A trade-off between the computation time and the precision has been reached using a relative error equal to 10^{-5}.

- Calculation of $\int_{k_0}^{\beta_p - \delta} F(\beta)d\beta$

In this interval, the complex function to be integrated has only the imaginary part and it is integrated using the DQDAGS subroutine.

- Calculation of $\int_{\beta_p-\delta}^{\beta_p+\delta} F(\beta)d\beta$

In this interval the complex function to be integrated has both the real and the imaginary parts. If the position of the pole is calculated with high precision, and if δ is made small, then the integral of the imaginary part is zero because the integral before the pole is equal and opposite to the integral after the pole. In our computation, we have calculated the pole position with an absolute precision of 10^{-12} rad/m and δ has been fixed at 10^{-4} rad/m .

The integral of the real part around the pole has been calculated analytically. To perform this calculation, we first write the function to be integrated in the form:

$$F(\beta) = \frac{f(\beta)}{T(\beta)} \tag{58}$$

where $f(\beta)$ is the non-singular portion of the function $F(\beta)$ and $T(\beta_p) = 0$. If small losses are introduced, the pole moves off the real β axis to $z_p = \beta_p + i\gamma_p$. Then, using the Taylor series expansion in the vicinity of the pole z_p, we can write $T(z) \cong T'(z_p)(z - z_p)$ where $T'(z_p) = \left.\frac{dT(z)}{dz}\right|_{z=z_p}$. In the vicinity of the pole the function $f(z)$ can also be approximated by $f(z_p)$ and the complex function to be integrated can be rewritten as:

$$F(z) \cong \frac{f(z_p)}{T'(z_p) \cdot (z - z_p)}. \tag{59}$$

As the integral will be performed along the real axis, we make $z = \beta$ in (59) and obtain

$$F(\beta) \cong \frac{f(\beta_p + i\gamma_p)}{T'(\beta_p + i\gamma_p) \cdot (\beta - \beta_p - i\gamma_p)}. \tag{60}$$

Consequently, an analytical solution for the integral is given by

$$\int_{\beta_p-\delta}^{\beta_p+\delta} F(\beta)d\beta = -\frac{f(\beta_p + i\gamma_p)}{T'(\beta_p + i\gamma_p)} \ln\left(\frac{i + \dfrac{\delta}{\gamma_p}}{i - \dfrac{\delta}{\gamma_p}}\right). \tag{61}$$

Furthermore, if we use the following identity

$$tg^{-1}(z) = \frac{i}{2} \ln \left(\frac{i+z}{i-z} \right) \tag{62}$$

equation (61) can be expressed as:

$$\int_{\beta_p-\delta}^{\beta_p+\delta} F(\beta) d\beta = 2i \; tg^{-1} \left(\frac{\delta}{\gamma_p} \right) \frac{f(\beta_p + i\gamma_p)}{T'(\beta_p + i\gamma_p)}. \tag{63}$$

For the lossless case $(\gamma_p = 0)$, we obtain:

$$\int_{\beta_p-\delta}^{\beta_p+\delta} F(\beta) d\beta = i\pi \frac{f(\beta_p)}{T'(\beta_p)}. \tag{64}$$

- Calculation of $\int_{\beta_p+\delta}^{b} F(\beta) d\beta$

In this interval, the function to be integrated is imaginary and the integral is calculated using the DQDAGS subroutine.

- Calculation of $\int_{b}^{+\infty} F(\beta) d\beta$

In this interval, the function to be integrated also has only the imaginary part. Using the method introduced in [27], we calculate through the DQDAGS subroutine the integrals

$$I_k = \int_{b}^{x_k} F(\beta) d\beta$$

where x_k is the k-th zero after b. Then we form the following sequences

$$M_1 = I_1$$
$$M_2 = \frac{I_1 + I_2}{2}$$

$$M_3 = \frac{I_1 + 2I_2 + I_3}{4}$$
$$\vdots$$
$$M_k = \frac{\sum_{m=1}^{k} \binom{k-1}{m-1} I_m}{2^{k-1}}. \tag{65}$$

According to [27], the required integral is given by:

$$\int_b^{+\infty} F(\beta)d\beta = \lim_{k\to+\infty} M_k. \tag{66}$$

In our numerical calculations, we have stopped the sequence when the relative difference between two consecutive terms was less than 10^{-6}.

6.1 Asymptotic Expression for the Imaginary Part of the Function to be Integrated

It can be shown that the imaginary part of the function to be integrated (equation (56)), when $\beta >> k_+$, is given by

$$\frac{i\omega \boldsymbol{I}\mu_0}{\pi}\sqrt{\frac{2}{\pi\rho}}\frac{1}{[p^2 + 2k_0^2(\varepsilon_r + 1)]}\beta^{3/2}\cos^2(\phi)\cos(\beta\rho - 0.25\pi)e^{+\beta(z-d)}. \tag{67}$$

When z is far from the interface $z = d$, the expression (67) shows that the oscillatory function $F(\beta)$ decreases swiftly when $\beta \to +\infty$ and the integral converges rapidly. This situation can be observed in Fig. 3 where we have plotted the imaginary part of $F(\beta)$ versus β for $x = 1.0d$, $y = 2.0d$, $z = 0.8d$, and $\xi_c = 1.0\,\mathrm{mS}$. It is also worth noting that the oscillatory function in the imaginary part of $F(\beta)$ has a period given by $T = 2\pi/\rho$. This property is shown in Fig. 4 for $\xi_c = 1.0\,\mathrm{mS}$, $y = 2.0d$, $z = 0.9d$, $x = 1.0d$ (continuous line), and $x = 5.0d$ (dashed line). The period for the continuous line is $87.8\,\mathrm{rad/m}$ while for the dashed line is $36.5\,\mathrm{rad/m}$.

However, when z is close to the interface the convergence is very slow. In the limiting case when $z = d$ the function diverges and this characteristic is presented in Fig. 5 for $x = 1.0d$, $y = 2.0d$, $z = d$, and $\xi_c = 1.0\,\mathrm{mS}$. The method introduced in [27] that uses the sequences

(65) allow to perform the integral also when $z = d$ and the function $F(\beta)$ diverges.

7. NUMERICAL RESULTS

Using the formulation described above, effects of chirality on near electromagnetic fields were analyzed in detail. We have chosen chiral admittance values normally found in the literature [8, 28] and, for brevity, only the results for the chirostrip structure with $\varepsilon_c = 2.0\varepsilon_0$, $d = 32.0$ mm, $\boldsymbol{I} = 1.0$ milliampere.meter, and $f = 2.0$ GHz are discussed below.

In Figs. 6, 7, and 8, we have drawn the polar plot of the electric field components $|\mathbf{E}_x|$, $|\mathbf{E}_y|$ and $|\mathbf{E}_z|$, computed for $z = 0.5d$, $\rho = 2.0d$ and two different values of chirality: $\xi_c = 1.0$ mS (continuous line) and 0.0mS (achiral substrate, dashed line). We note that, when the chirality is present, there is no symmetry with respect to the x-z plane containing the short dipole because the chirality causes a rotation in the near field structure. Another way to visualize this effect is presented in Fig. 9, where we have plotted the magnitude of $\mathbf{E}_z$ component versus x/d with $y = 2.0d$ and $z = 0.7d$. Clearly, the rotation caused by the chirality modifies the symmetry of the field distribution with respect to the $x = 0$ plane. This phenomenon has been previously reported only for the far field region [17].

In Fig. 10, we have drawn the magnitude of the z-component of the magnetic field as a function of z/d with $x = 1.0d$, $y = 2.0d$, and for two different values of chirality: $\xi_c = 1.0$ mS (continuous line) and 0.0mS (achiral substrate, dashed line). We note that, when the chirality is present, the magnetic field component $\mathbf{H}_z$ is not zero on the perfectly conducting surface $z = 0$ and it is also discontinuous on the interface $z = d$, in spite of the magnetic permeability being the same on the two sides of the interface. This is an intrinsic characteristic of chiral media. Of course the z-component of the magnetic flux density vector $\vec{\mathbf{B}}$ is zero at the interface $z = 0$ and is continuous at the interface $z = d$ even when the chirality is different from zero, as it can be seen in Fig. 11.

The discontinuity in the z-component of the magnetic field at the interface $z = d$ is further analyzed in Fig. 12, where we show the plots of $\mathbf{H}_{z_0}$ and $\mathbf{H}_z$. The continuous line is the z-component of the magnetic field in the chiral substrate and the dashed line is the same component in the free space region. The parameters are $\xi_c = 1.0$ mS and $\rho = 2.0d$. In this figure, we also observe that the $\mathbf{H}_z$ component

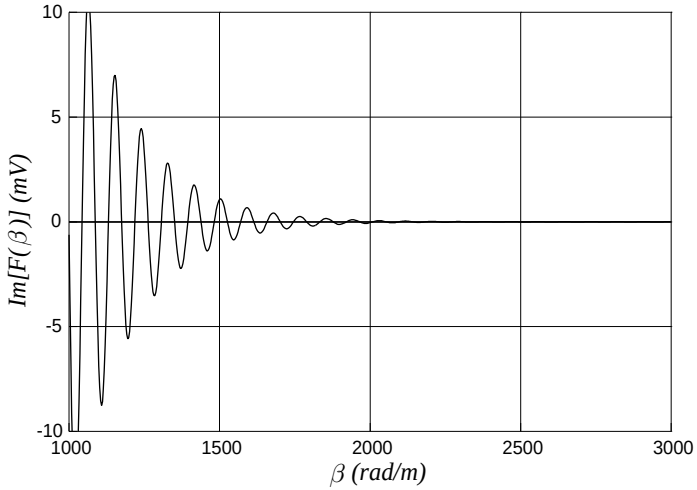

Figure 3. Imaginary part of the complex function $F(\beta)$ that must be integrated to obtain the electric field component $\mathbf{E}_x(x, y, z)$ in the chiral substrate, computed for $f = 2.0\,\mathrm{GHz}$, $\boldsymbol{I} = 1.0\,\mathrm{milliampere.meter}$, $\varepsilon_c = 2.0\varepsilon_0$, $d = 32.0\,\mathrm{mm}$, $\xi_c = 1.0\,\mathrm{mS}$, $x = 1.0d$, $y = 2.0d$, and $z = 0.8d$.

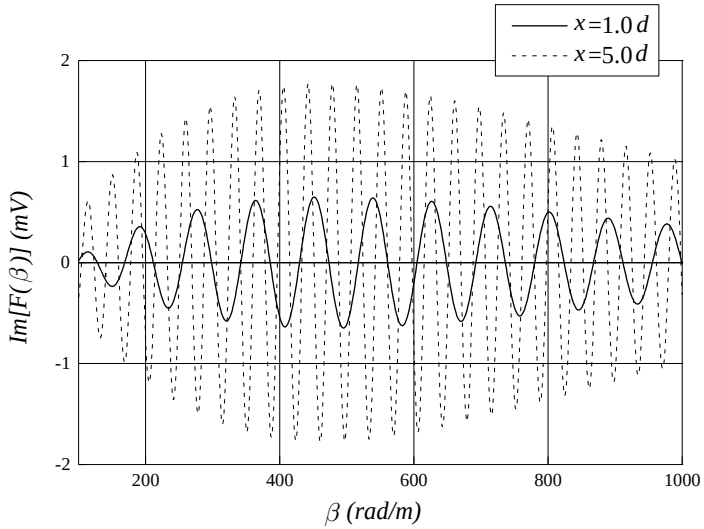

Figure 4. Imaginary part of the complex function $F(\beta)$ that must be integrated to obtain the electric field component $\mathbf{E}_x(x, y, z)$ in the chiral substrate, computed for $f = 2.0\,\mathrm{GHz}$, $\boldsymbol{I} = 1.0\,\mathrm{milliampere.meter}$, $\varepsilon_c = 2.0\varepsilon_0$, $d = 32.0\,\mathrm{mm}$, $\xi_c = 1.0\,\mathrm{mS}$, $y = 2.0d$, $z = 0.9d$, and two different values of x : $1.0d$ (continuous line) and $5.0d$ (dashed line).

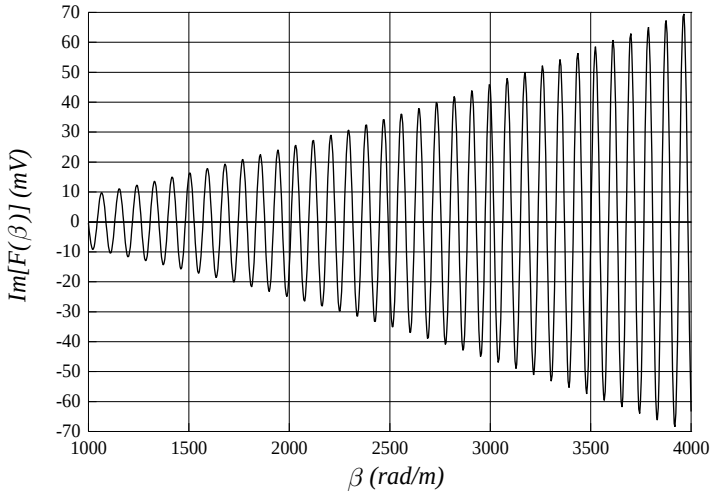

Figure 5. Imaginary part of the complex function $F(\beta)$ that must be integrated to obtain the electric field component $\mathbf{E}_x(x, y, z)$ at the planar interface $z = 1.0d$, computed for $f = 2.0\,\text{GHz}$, $\boldsymbol{I} = 1.0\,\text{milliampere.meter}, \varepsilon_c = 2.0\varepsilon_0$, $d = 32.0\,\text{mm}$, $\xi_c = 1.0\,\text{mS}$, $x = 1.0d$, and $y = 2.0d$.

rotates by an angle different than that of $\mathbf{H}_{z_0}$. The difference between these two angles in this particular case is 6 degrees. This phenomenon has been verified by the authors in [23].

8. CONCLUSIONS

In this paper, a dynamic model to calculate the near electromagnetic fields excited by a short dipole printed on a grounded chiral slab is presented. As the calculation is carried out in the Fourier domain, we obtain the spectral electromagnetic fields in compact and closed forms where only sine and cosine functions are present. This is a very efficient approach for the numerical calculation of the electromagnetic fields in the space domain through double integrals in the spectral plane. Effects of chirality on near field distributions were presented and discussed. As a result of our calculation we clearly noticed that the chirality can cause a rotation in the near field structure and, consequently, in the far field pattern. Then, we can state that, at the interface between a perfectly conducting surface and a chiral substrate, the

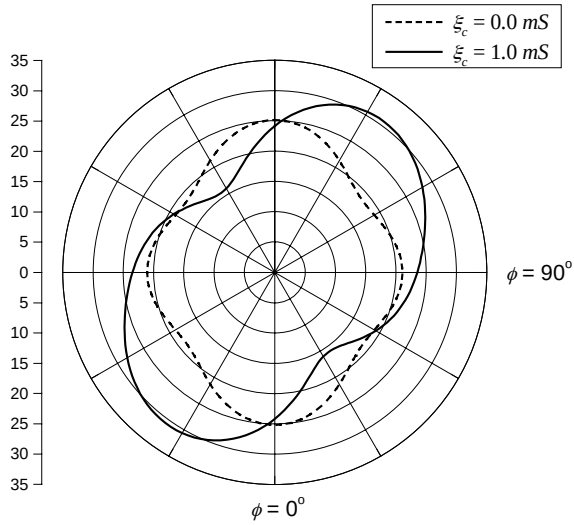

Figure 6. Polar plot of the electric field component $|\mathbf{E}_x|$, expressed in volt/m, computed for $f = 2.0\,\text{GHz}$, $\boldsymbol{I} = 1.0\,\text{milliampere.meter}$, $\varepsilon_c = 2.0\varepsilon_0$, $d = 32.0\,\text{mm}$, $z = 0.5d$, $\rho = 2.0d$, and two different values of chirality: $\xi_c = 1.0\,\text{mS}$ (continuous line) and $0.0\,\text{mS}$ (achiral substrate, dashed line).

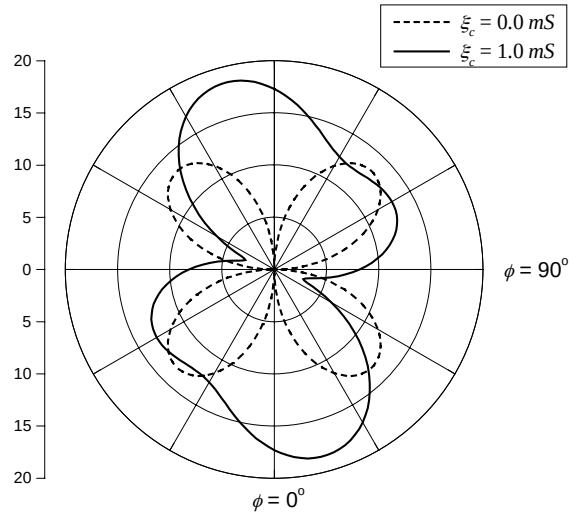

Figure 7. Polar plot of the electric field component $|\mathbf{E}_y|$, expressed in volt/m, computed for $f = 2.0\,\text{GHz}$, $\boldsymbol{I} = 1.0\,\text{milliampere.meter}$, $\varepsilon_c = 2.0\varepsilon_0$, $d = 32.0\,\text{mm}$, $z = 0.5d$, $\rho = 2.0d$, and two different values of chirality: $\xi_c = 1.0\,\text{mS}$ (continuous line) and $0.0\,\text{mS}$ (achiral substrate, dashed line).

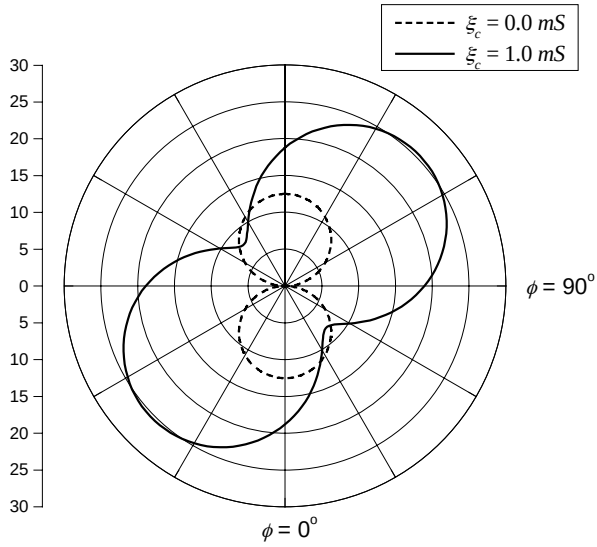

Figure 8. Polar plot of the electric field component $|\mathbf{E}_z|$, expressed in volt/m, computed for $f = 2.0\,\text{GHz}$, $\boldsymbol{I} = 1.0\,\text{milliampere.meter}$, $\varepsilon_c = 2.0\varepsilon_0$, $d = 32.0\,\text{mm}$, $z = 0.5d$, $\rho = 2.0d$, and two different values of chirality: $\xi_c = 1.0\,\text{mS}$ (continuous line) and $0.0\,\text{mS}$ (achiral substrate, dashed line).

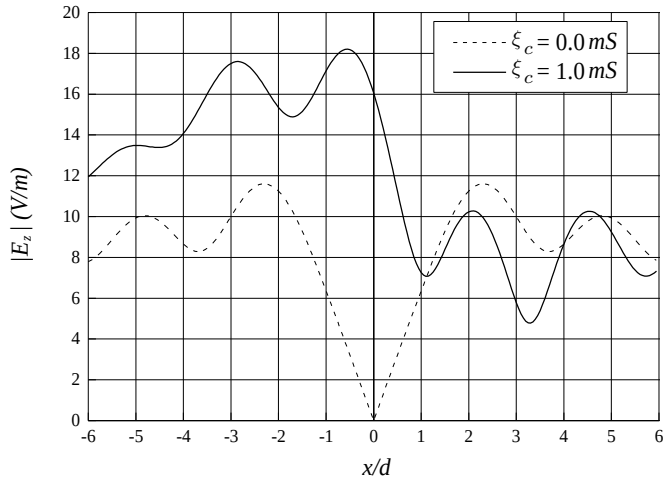

Figure 9. Amplitude (absolute value) of the electric field component $\mathbf{E}_z$ versus x/d, expressed in volt/m, computed for $f = 2.0\,\text{GHz}$, $\boldsymbol{I} = 1.0\,\text{milliampere.meter}$, $\varepsilon_c = 2.0\varepsilon_0$, $d = 32.0\,\text{mm}$, $y = 2.0d$, $z = 0.7d$, and two different values of chirality: $\xi_c = 1.0\,\text{mS}$ (continuous line) and $0.0\,\text{mS}$ (achiral substrate, dashed line).

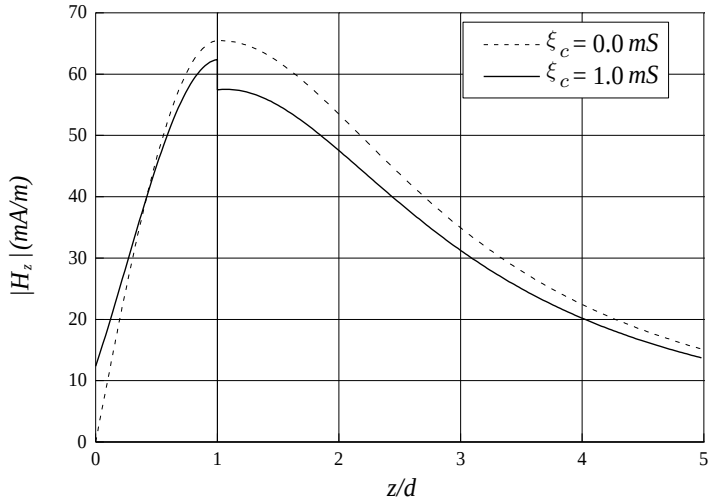

Figure 10. Amplitude (absolute value) of the magnetic field component $\mathbf{H}_z$ versus z/d, expressed in m.A/m, computed for $f = 2.0\,\mathrm{GHz}$, $\boldsymbol{I} = 1.0$ milliampere.meter, $\varepsilon_c = 2.0\varepsilon_0$, $d = 32.0\,\mathrm{mm}$, $x = 1.0d$, $y = 2.0d$, and two different values of chirality: $\xi_c = 1.0\,\mathrm{mS}$ (continuous line) and $0.0\,\mathrm{mS}$ (achiral substrate, dashed line).

magnetic field component normal to this surface is not null. Moreover, at the interface between the chiral substrate and the free space, the magnetic field component normal to this surface is not continuous even when the magnetic permeability is the same in the two media. The numerical technique developed in this work has potential applications in microwave and millimeter wave circuit components, printed antennas and integrated optics.

9. APPENDIX

9.1 Transformed Electromagnetic Fields Inside the Chiral Substrate

The expressions for the components of the transformed electromagnetic fields inside the chiral substrate $(0 < z < d)$ are shown below. We remember that the expression of $\boldsymbol{\mathcal{E}}_x(k_x, k_y, z)$ has already been given in the body of this paper.

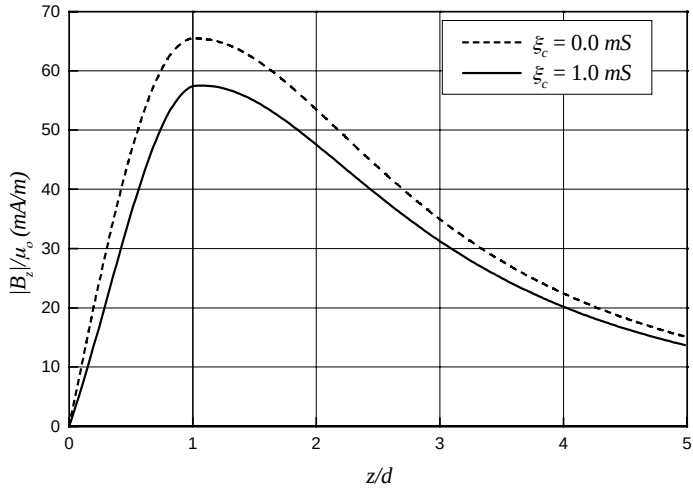

Figure 11. Amplitude (absolute value) of the magnetic flux density component $\mathbf{B}_z$ versus z/d, computed for $f = 2.0\,\mathrm{GHz}$, $\boldsymbol{I} = 1.0\,\mathrm{milliampere.meter}$, $\varepsilon_c = 2.0\varepsilon_0$, $d = 32.0\,\mathrm{mm}$, $x = 1.0d$, $y = 2.0d$, and two different values of chirality: $\xi_c = 1.0\,\mathrm{mS}$ (continuous line) and $0.0\,\mathrm{mS}$ (achiral substrate, dashed line). In this figure $(|\mathbf{B}_z|/\mu_0)$ is expressed in m.A/m.

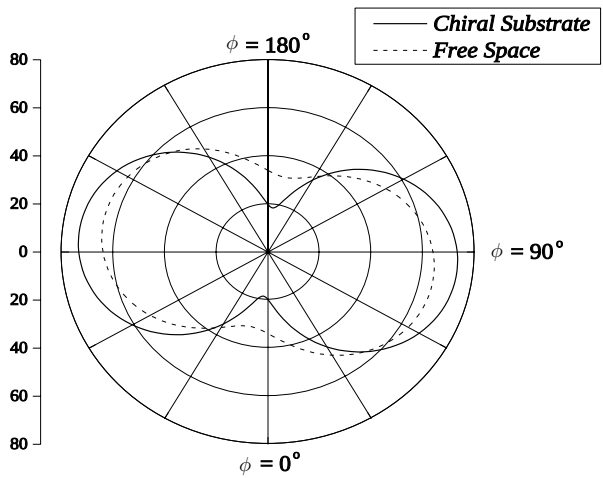

Figure 12. Polar plot of the magnetic field component $\mathbf{H}_z$, expressed in m.A/m, at the interface between the chiral substrate and free space region, computed for $f = 2.0\,\mathrm{GHz}$, $\boldsymbol{I} = 1.0\,\mathrm{milliampere.meter}$, $\varepsilon_c = 2.0\varepsilon_0$, $d = 32.0\,\mathrm{mm}, \rho = 2.0d$, and $\xi_c = 1.0\,\mathrm{mS}$. The continuous line is the z-component in the chiral substrate side and the dashed line is the same component in the free space region side.

$$\boldsymbol{\mathcal{E}}_y(k_x,k_y,z) = \frac{\omega \boldsymbol{I}\mu_0}{2u^2\Delta(u^2)}\Big[N_{xx}^{(c)}(z,u^2)k_x^2 + N_{xy}^{(c)}(z,u^2)k_xk_y + N_{yy}^{(c)}(z,u^2)k_y^2\Big] \tag{68}$$

where

$$\begin{aligned} N_{xx}^{(c)}(z,u^2) = &- ik_c^2\left[\cos(\gamma_1 z) - \cos(\gamma_2 z)\right]B_x \\ &- z\left[k_+\,\mathrm{sinc}(\gamma_1 z) + k_-\,\mathrm{sinc}(\gamma_2 z)\right]A_x \end{aligned} \tag{69}$$

$$\begin{aligned} N_{xy}^{(c)}(z,u^2) = &\left(A_x - ik_c^2 B_y\right)\left[\cos(\gamma_1 z) - \cos(\gamma_2 z)\right] \\ &- z\left[k_+A_y + ik_-\gamma_1^2 B_x\right]\,\mathrm{sinc}(\gamma_1 z) \\ &- z\left[k_-A_y + ik_+\gamma_2^2 B_x\right]\,\mathrm{sinc}(\gamma_2 z) \end{aligned} \tag{70}$$

$$\begin{aligned} N_{yy}^{(c)}(z,u^2) = &\left[\cos(\gamma_1 z) - \cos(\gamma_2 z)\right]A_y \\ &- iz\left[k_-\gamma_1^2\,\mathrm{sinc}(\gamma_1 z) + k_+\gamma_2^2\,\mathrm{sinc}(\gamma_2 z)\right]B_y \end{aligned} \tag{71}$$

$$\boldsymbol{\mathcal{E}}_z(k_x,k_y,z) = \frac{\omega \boldsymbol{I}\mu_0}{2\Delta(u^2)}\left[M_x^{(c)}(z,u^2)k_x + M_y^{(c)}(z,u^2)k_y\right] \tag{72}$$

where

$$\begin{aligned} M_x^{(c)}(z,u^2) = &- \left[k_-\cos(\gamma_1 z) + k_+\cos(\gamma_2 z)\right]B_x \\ &+ iz\left[\,\mathrm{sinc}(\gamma_1 z) - \,\mathrm{sinc}(\gamma_2 z)\right]A_x \end{aligned} \tag{73}$$

$$\begin{aligned} M_y^{(c)}(z,u^2) = &- \left[k_-\cos(\gamma_1 z) + k_+\cos(\gamma_2 z)\right]B_y \\ &+ iz\left[\,\mathrm{sinc}(\gamma_1 z) - \,\mathrm{sinc}(\gamma_2 z)\right]A_y \end{aligned} \tag{74}$$

$$\boldsymbol{\mathcal{H}}_x(k_x,k_y,z) = \frac{-q\boldsymbol{I}}{2u^2\Delta(u^2)}\Big[S_{xx}^{(c)}(z,u^2)k_x^2 + S_{xy}^{(c)}(z,u^2)k_xk_y + S_{yy}^{(c)}(z,u^2)k_y^2\Big] \tag{75}$$

where

$$\begin{aligned} S_{xx}^{(c)}(z,u^2) = &- i\left[\cos(\gamma_1 z) + \cos(\gamma_2 z)\right]A_x \\ &- z\left[k_-\gamma_1^2\,\mathrm{sinc}(\gamma_1 z) - k_+\gamma_2^2\,\mathrm{sinc}(\gamma_2 z)\right]B_x \end{aligned} \tag{76}$$

$$\begin{aligned} S_{xy}^{(c)}(z,u^2) = &\left(-iA_y + k_c^2 B_x\right)\left[\cos(\gamma_1 z) + \cos(\gamma_2 z)\right] \\ &- z(ik_+A_x + k_-\gamma_1^2 B_y)\,\mathrm{sinc}(\gamma_1 z) \end{aligned}$$

$$+ z(ik_- A_x + k_+\gamma_2^2 B_y)\,\mathrm{sinc}(\gamma_2 z) \tag{77}$$

$$S_{yy}^{(c)}(z,u^2) = k_c^2\left[\cos(\gamma_1 z) + \cos(\gamma_2 z)\right] B_y - iz\left[k_+\,\mathrm{sinc}(\gamma_1 z) - k_-\,\mathrm{sinc}(\gamma_2 z)\right] A_y \tag{78}$$

$$\boldsymbol{\mathcal{H}}_y(k_x,k_y,z) = \frac{-q\boldsymbol{I}}{2u^2\Delta(u^2)}\left[T_{xx}^{(c)}(z,u^2)k_x^2 + T_{xy}^{(c)}(z,u^2)k_x k_y + T_{yy}^{(c)}(z,u^2)k_y^2\right] \tag{79}$$

where

$$T_{xx}^{(c)}(z,u^2) = -k_c^2\left[\cos(\gamma_1 z) + \cos(\gamma_2 z)\right] B_x + iz\left[k_+\,\mathrm{sinc}(\gamma_1 z) - k_-\,\mathrm{sinc}(\gamma_2 z)\right] A_x \tag{80}$$

$$T_{xy}^{(c)}(z,u^2) = (-iA_x - k_c^2 B_y)\left[\cos(\gamma_1 z) + \cos(\gamma_2 z)\right] + z(ik_+ A_y - k_-\gamma_1^2 B_x)\,\mathrm{sinc}(\gamma_1 z) - z(ik_- A_y - k_+\gamma_2^2 B_x)\,\mathrm{sinc}(\gamma_2 z) \tag{81}$$

$$T_{yy}^{(c)}(z,u^2) = -i\left[\cos(\gamma_1 z) + \cos(\gamma_2 z)\right] A_y - z\left[k_-\gamma_1^2\,\mathrm{sinc}(\gamma_1 z) - k_+\gamma_2^2\,\mathrm{sinc}(\gamma_2 z)\right] B_y \tag{82}$$

$$\boldsymbol{\mathcal{H}}_z(k_x,k_y,z) = \frac{-q\boldsymbol{I}}{2\Delta(u^2)}\left[S_x^{(c)}(z,u^2)k_x + S_y^{(c)}(z,u^2)k_y\right] \tag{83}$$

where

$$S_x^{(c)}(z,u^2) = i\left[k_-\cos(\gamma_1 z) - k_+\cos(\gamma_2 z)\right] B_x + z\left[\mathrm{sinc}(\gamma_1 z) + \mathrm{sinc}(\gamma_2 z)\right] A_x \tag{84}$$

$$S_y^{(c)}(z,u^2) = i\left[k_-\cos(\gamma_1 z) - k_+\cos(\gamma_2 z)\right] B_y + z\left[\mathrm{sinc}(\gamma_1 z) + \mathrm{sinc}(\gamma_2 z)\right] A_y \tag{85}$$

9.2 Transformed Electromagnetic Fields in the Free Space Region

The expressions for the components of the transformed electromagnetic fields in the free space region $(z > d)$ are shown below. We remember that the expression of $\boldsymbol{\mathcal{E}}_{x_0}(k_x,k_y,z)$ has already been given in the body of this paper.

$$\boldsymbol{\mathcal{E}}_{y_0}(k_x,k_y,z) = \frac{\omega\boldsymbol{I}\mu_0 e^{ik_{z0}(d-z)}}{\Delta(u^2)}\left[N_{xx}^{(0)}(u^2)(k_x^2 - k_y^2) + N_{xy}^{(0)}(u^2)k_x k_y\right] \tag{86}$$

where

$$N_{xx}^{(0)}(u^2) = -2ipd^2q^2k_{z0}\,\mathrm{sinc}(\gamma_1 d)\,\mathrm{sinc}(\gamma_2 d) \tag{87}$$

$$\begin{aligned} N_{xy}^{(0)}(u^2) = &-k_c^2\left[1-\cos(\gamma_1 d)\cos(\gamma_2 d)\right] \\ &+ iqdk_{z0}\left[k_+\cos(\gamma_1 d)\,\mathrm{sinc}(\gamma_2 d)\right. \\ &+ \left.k_-\cos(\gamma_2 d)\,\mathrm{sinc}(\gamma_1 d)\right] \\ &- 0.5d^2(k_+^2\gamma_2^2 + k_-^2\gamma_1^2)\,\mathrm{sinc}(\gamma_1 d)\,\mathrm{sinc}(\gamma_2 d) \end{aligned} \tag{88}$$

$$\boldsymbol{\mathcal{E}}_{z_0}(k_x,k_y,z) = \frac{-\omega \boldsymbol{I}\mu_0 e^{ik_{z0}(d-z)}}{\Delta(u^2)}\left[M_x^{(0)}(u^2)k_x + M_y^{(0)}(u^2)k_y\right] \tag{89}$$

where

$$\begin{aligned} M_x^{(0)}(u^2) = &\,k_c^2k_{z0}\left[1-\cos(\gamma_1 d)\cos(\gamma_2 d)\right] \\ &- iqd\left[k_+\gamma_2^2\cos(\gamma_1 d)\,\mathrm{sinc}(\gamma_2 d)\right. \\ &+ \left.k_-\gamma_1^2\cos(\gamma_2 d)\,\mathrm{sinc}(\gamma_1 d)\right] \\ &+ 0.5d^2k_{z0}(k_+^2\gamma_2^2 + k_-^2\gamma_1^2)\,\mathrm{sinc}(\gamma_1 d)\,\mathrm{sinc}(\gamma_2 d) \end{aligned} \tag{90}$$

$$M_y^{(0)}(u^2) = 2ipd^2q^2u^2\,\mathrm{sinc}(\gamma_1 d)\,\mathrm{sinc}(\gamma_2 d) \tag{91}$$

$$\begin{aligned} \boldsymbol{\mathcal{H}}_{x_0}(k_x,k_y,z) = &\frac{-i\boldsymbol{I}e^{ik_{z0}(d-z)}}{u^2\Delta(u^2)}\left[S_{xx}^{(0)}(u^2)k_x^2 + S_{xy}^{(0)}(u^2)k_xk_y\right. \\ &+ \left.S_{yy}^{(0)}(u^2)k_y^2\right] \end{aligned} \tag{92}$$

where

$$S_{xx}^{(0)}(u^2) = -2pd^2q^2u^2k_{z0}^2\,\mathrm{sinc}(\gamma_1 d)\,\mathrm{sinc}(\gamma_2 d) \tag{93}$$

$$\begin{aligned} S_{xy}^{(0)}(u^2) = &\,qd(-k_0^2\gamma_2^2k_+ + k_{z0}^2k_c^2k_-)\cos(\gamma_1 d)\,\mathrm{sinc}(\gamma_2 d) \\ &+ qd(-k_0^2\gamma_1^2k_- + k_{z0}^2k_c^2k_+)\cos(\gamma_2 d)\,\mathrm{sinc}(\gamma_1 d) \end{aligned} \tag{94}$$

$$S_{yy}^{(0)}(u^2) = 2pd^2q^2u^2k_0^2\,\mathrm{sinc}(\gamma_1 d)\,\mathrm{sinc}(\gamma_2 d) \tag{95}$$

$$\begin{aligned} \boldsymbol{\mathcal{H}}_{y_0}(k_x,k_y,z) = &\frac{\boldsymbol{I}e^{ik_{z0}(d-z)}}{u^2\Delta(u^2)}\left[T^{(0)}(u^2) + T_{xx}^{(0)}(u^2)k_x^2\right. \\ &+ \left.T_{xy}^{(0)}(u^2)k_xk_y + T_{yy}^{(0)}(u^2)k_y^2\right] \end{aligned} \tag{96}$$

where

$$T^{(0)}(u^2) = u^2 \left[k_0^2 k_{z0} k_c^2 [1 - \cos(\gamma_1 d)\cos(\gamma_2 d)] + 0.5 d^2 k_0^2 k_{z0} (k_+^2 \gamma_2^2 + k_-^2 \gamma_1^2) \operatorname{sinc}(\gamma_1 d) \operatorname{sinc}(\gamma_2 d)\right] \quad (97)$$

$$T_{xx}^{(0)}(u^2) = -iqdk_0^2 \left[k_+ \gamma_2^2 \cos(\gamma_1 d) \operatorname{sinc}(\gamma_2 d) + k_- \gamma_1^2 \cos(\gamma_2 d) \operatorname{sinc}(\gamma_1 d)\right] \quad (98)$$

$$T_{xy}^{(0)}(u^2) = 2ipd^2 q^2 u^2 (k_0^2 + k_{z0}^2) \operatorname{sinc}(\gamma_1 d) \operatorname{sinc}(\gamma_2 d) \quad (99)$$

$$T_{yy}^{(0)}(u^2) = -iqdk_{z0}^2 k_c^2 \left[k_- \cos(\gamma_1 d) \operatorname{sinc}(\gamma_2 d) + k_+ \cos(\gamma_2 d) \operatorname{sinc}(\gamma_1 d)\right] \quad (100)$$

$$\boldsymbol{\mathcal{H}}_{z_0}(k_x, k_y, z) = \frac{-\boldsymbol{I} e^{ik_{z0}(d-z)}}{\Delta(u^2)} \left[S_x^{(0)}(u^2) k_x + S_y^{(0)}(u^2) k_y\right] \quad (101)$$

where

$$S_x^{(0)}(u^2) = 2ipd^2 q^2 u^2 k_{z0} \operatorname{sinc}(\gamma_1 d) \operatorname{sinc}(\gamma_2 d) \quad (102)$$

$$S_y^{(0)}(u^2) = k_c^2 k_0^2 [1 - \cos(\gamma_1 d)\cos(\gamma_2 d)] - iqdk_c^2 k_{z0} [k_- \cos(\gamma_1 d) \operatorname{sinc}(\gamma_2 d) + k_+ \cos(\gamma_2 d) \operatorname{sinc}(\gamma_1 d)] + 0.5 d^2 k_0^2 (k_+^2 \gamma_2^2 + k_-^2 \gamma_1^2) \operatorname{sinc}(\gamma_1 d) \operatorname{sinc}(\gamma_2 d) \quad (103)$$

ACKNOWLEDGMENT

This work was partially supported by the Brazilian Research Council (CNPq) under Grant 521049/94–6.

REFERENCES

1. Bassari, S., C. H. Papas, and N. Engheta, "Electromagnetic wave propagation through a dielectric-chiral interface and through a chiral slab," *J. Opt. Soc. Am. A.,* Vol. 5, No. 9, 1450–1459, 1988. Errata: Vol. 7, No. 11, 2154–2155, 1990.
2. Engheta, N., and P. Pelet, "Modes in chirowaveguides," *Opt. Lett.,* Vol. 14, No. 11, 593–595, 1989.
3. Pelet, P., and N. Engheta, "The theory of chirowaveguides," *IEEE Trans. Antennas Prop.,* Vol. 38, No. 1, 90–98, 1990.
4. Engheta, N., and P. Pelet, "Surface waves in chiral layers," *Opt. Lett.,* Vol. 16, No. 10, 723–725, 1991.

5. Paiva, C. R., and A. M. Barbosa, "A method for the analysis of bi-isotropic planar waveguides: application to a grounded chiroslabguide," *Electromagnetics,* Vol. 11, 209–221, 1991.
6. Cory, H. and I. Rosenhouse, "Electromagnetic wave propagation along a chiral slab," *IEE Proc. Pt. -H, Microwave, Antennas, Propagation,* Vol. 138, No. 1, 51–54, 1991.
7. Mariotte, F., P. Pelet, and N. Engheta, "A review of recent study of guided waves in chiral media," *Progress in Electromagnetics Research (PIER),* Vol. 9 on Bianisotropic and Bi-isotropic Media and Applications, A. Priou (Ed.), Chapter 12, 311–350, EMW Publishing, Cambridge, Massachusetts, 1994.
8. Cory, H., "Chiral devices – an overview of canonical problems," *J. Electromagn. Waves Appl.,* Vol. 9, No. 5/6, 805–829, 1995.
9. Lacava, J. C. S., and F. Lumini, "An alternative formulation for guided electromagnetic fields in grounded chiral slabs," *Progress in Electromagnetics Research (PIER),* Vol. 16 on Electromagnetic Waves, J. A. Kong (Ed.), Chapter 11, 285–304, EMW Publishing, Cambridge, Massachusetts, 1997.
10. Plaza, G., F. Mesa, and M. Horno, "Study of the dispersion characteristics of planar chiral lines," *IEEE Trans. Microwave Theory Techn.,* Vol. 46, No. 8, 1150–1157, 1998.
11. Pelet, P., and N. Engheta, "Chirostrip antenna: line source problem," *J. Electromagn. Waves Appl.,* Vol. 6, No. 5/6, 771–793, 1992.
12. Cheng, D., and L. Xue, "Dipole radiation in the presence of a grounded chiral slab," *J. Electromagn. Waves Appl.,* Vol. 5, No. 2, 65–68, 1992.
13. Toscano, L., and L. Vegni, "Spectral dyadic Green's function formulation for planar integrated structures with a grounded chiral slab," *J. Electromagn. Waves Appl.,* Vol. 6, No. 5/6, 751–769, 1992.
14. Lumini, F., and J. C. S. Lacava, "Radiation properties of chirostrip antennas," *Proceedings of the 1993 SBMO International Microwave Conference,* Vol. 2, 587–592, São Paulo, Brazil, August 1993.
15. Pelet, P., and N. Engheta, "Theoretical study of radiation properties of a finite-length thin-wire chirostrip antenna using dyadic Green's functions and method of moments," *Progress in Electromagnetics Research (PIER),* Vol. 9 on Bianisotropic and Biisotropic Media and Applications. A. Priou (Ed.), Chapter 14, 265–288, EMW Publishing, Cambridge, Massachusetts, 1994.
16. Lumini, F., and J. C. S. Lacava, "Electromagnetic fields in open chirostrip multilayered structures," *Proceedings of the 1997*

SBMO/IEEE MTT-S International Microwave and Optoelectronics Conference, Vol. 2, 649–654, Natal, Brazil, August 1997.

17. Pelet, P., and N. Engheta, "Novel rotational characteristics of radiation patterns of chirostrip dipole antennas," *Microwave Opt. Technol. Lett.,* Vol. 5, No. 1, 31–34, 1992.
18. Pelet, P., and N. Engheta, "Mutual coupling in finite-length thin wire chirostrip antennas," *Microwave Opt. Technol. Lett.,* Vol. 6, No. 12, 671–675, 1993.
19. Pozar, D. M., "Microstrip antennas and arrays on chiral substrates," *IEEE Trans. Antennas Prop.,* Vol. 40, No. 10, 1260–1263, 1992.
20. Toscano, A., and L. Vegni, "A new efficient moment method formulation for the design of microstrip antennas over a chiral grounded slab," *J. Electromagn. Waves Appl.,* Vol. 11, No. 5, 567–592, 1997.
21. Unrau, U. B., "A bibliography on research in the field of bi-anisotropic, bi-isotropic and chiral media and their microwave applications," *Proceedings of CHIRAL'94: 3rd International Workshop on Chiral, Bi-isotropic and Bi-anisotropic Media,* A1–A48, Périgueux, France, 1994. The bibliography is also available in electronic form from the Listserv group CHIRAL-L.
22. Lumini, F., and J. C. S. Lacava, "Numerical calculation of electromagnetic fields in multilayered chirostrip antennas," *Proceedings of the* 11^{th} *Conference on the Computation of Electromagnetic Fields,* Vol. 2, 675–676, Rio de Janeiro, Brazil, November 1997.
23. Lumini, F., and J. C. S. Lacava, "On the behavior of electromagnetic fields on the interfaces of chirostrip dipole antennas," *Microwave Opt. Technol. Lett.,* Vol. 19, No. 5, 338–342, 1998.
24. Scott, C., *The Spectral Domain Method in Electromagnetics,* Artech House, Norwood, 1989.
25. Sihvola, A. H., and I. V. Lindell, "Bi-isotropic constitutive relations," *Microwave Opt. Technol. Lett.,* Vol. 4, No. 8, 295–297, July 1991.
26. McLachlan, N. W., *Bessel Functions for Engineers,* Oxford University Press, London, 1941.
27. Mosig, J. R., and F. Gardiol, "Analytical and numerical techniques for the analysis of microstrip antennas," *Ann. Télécommun.,* Vol. 40, No. 7–8, 411–437, 1985.
28. Ougier, S., I. Chenerie, and S. Bolioli, "Measurement method for chiral media," *Proceedings of the 22nd European Microwave Conference,* Vol. 1, 682–687, Espoo, Finland, August 1992.